

Experiment research on seismic performance of prestressed steel reinforced high performance concrete beams

Weichen Xue*, Feng Yang and Liang Li

Department of Building Engineering, Tongji University, Shanghai, China

(Received October 28, 2007, Accepted December 18, 2008)

Abstract. Two prestressed steel reinforced high performance concrete (SRC) beams, a nonprestressed SRC beam and a counterpart prestressed concrete beam were tested under low reversed cyclic loading to evaluate seismic performance of prestressed SRC beams. The failure modes, deformation restoring capacity, ductility and energy dissipation capacity of the prestressed SRC beams were discussed. Results showed that due to the effect of plastic deformations of steel beams encased in concrete, the three SRC beams exhibited residual deformation ratios ranging between 0.64 and 0.79, which were apparently higher than that of the prestressed concrete beam (0.33). The ductility coefficients of the prestressed SRC beams and the prestressed concrete beam ranged between 4.65 and 4.87, obviously lower than that of nonprestressed SRC beam (9.09), which indicated the steel beams influenced the ductility little while prestressing resulted in an apparent reduction in ductility. The amount of energy dissipated by the prestressed SRC beams was less than that dissipated by the nonprestressed SRC beam but much more than that dissipated by the prestressed concrete beam.

Keywords: steel reinforced concrete beam; prestressing; seismic performance; ductility; deformation restoring capacity; energy dissipation.

1. Introduction

Steel reinforced concrete (SRC) structures have been used in large span structures and high-rise buildings in seismic regions due to large global stiffness, high load-carrying capacity, ductility and energy dissipation capacity. Compared with nonprestressed SRC structures, prestressed SRC structures demonstrate many advantages, such as a reduction in concrete cracking and structural deformation and an increment in load-carrying capacity.

Studies on SRC structures have been carried out in many countries, such as Japan, England, America and China and previous studies mainly focused on nonprestressed SRC structures. Investigations have been carried out to study static behaviors (Lu 2006, Teraoka *et al.* 2001) and seismic performance (Azizinamini and Ghosh 1997, Chen and Lin 2008, Cheng and Chung 2002, Chou and Uang 2001, Lee and Pan 2001, Xue and Zhao 2000, Wakabayashi 1986) of nonprestressed SRC structures. Design methods for SRC structures have also been proposed. However, only a little attention (Sun *et al.* 1996) has been paid to static behaviors of prestressed SRC structures and hardly no has been paid to seismic performance of prestressed SRC structures.

* Corresponding Author, Email: xuewc@mail.tongji.edu.cn

This paper aims to study seismic performance of prestressed SRC beams under low reversed cyclic loading. The failure modes, deformation restoring capacity, ductility and energy dissipation capacity of prestressed SRC beams are discussed in this paper.

2. Test setup

2.1 Specimens design

Two prestressed SRC beam specimens, which were denoted as PSRCB-1 and PSRCB-2 and two reference specimens denoted as PHPCB and SRCB, were designed in identical dimensions, with clear span of 4200 mm, width of 200 mm and depth of 300 mm. Here, PHPCB was a prestressed concrete beam and SRCB was a nonprestressed SRC beam. PSRCB1 and PSRCB-2 were prestressed with partial prestressing ratios (PPR) of 0.75 and 0.85, respectively. Note that the PPR was defined as:

$$PPR = \frac{A_p f_{py}}{A_p f_{py} + A_s f_y}$$

where A_p is the cross-section area of the prestressing tendon; A_s is the cross-section area of the longitudinal reinforcement; f_{py} is the yield strength of the prestressing tendon; and f_y is the yield strength of the longitudinal reinforcement.

Eight steel wires with diameter of 5 mm were placed in PSRCB-1 and two steel strands with diameter of 15 mm were placed in PSRCB-2. Studs with diameter of 16 mm were welded to steel beams, with spacing of 400 mm in pure bending sections and 200 mm in flexure-shear sections. Low relaxation steel wires and strands with ultimate strength of 1860 MPa were used as bonded prestressing bars. The jacking stress σ_{con} was equal to 1395 MPa. All beams were post-tensioned at one end. The jacking process was: $0 \rightarrow 0.1\sigma_{con} \rightarrow 0.2\sigma_{con} \rightarrow 0.6\sigma_{con} \rightarrow 1.0\sigma_{con} \rightarrow 1.03\sigma_{con} \rightarrow$ keeping the load constant for two minutes \rightarrow anchoring. The measured effective stress for the prestressing tendons in mid-span sections of PHPCB was about 1122 MPa and in PSRCB-1 and PSRCB-2 about 1069 MPa.

Details of the specimens are listed in Table 1. All specimens were cast with C50 high performance concrete (HPC). The added grinded blast furnace slags in concrete with fineness of $5 \times 10^3 \text{ cm}^2/\text{g}$ were used to replace part of cement for strengthening the activity of admixtures. The adding of polypropylene fibers (15 mm in length) with 2.3% volume fraction of cement was an attempt to increase the anti-dry-shrinkage cracking property of cement mortar in hardening stage. Content of cement, grinded blast furnace slags, water, middle grit, gravels, fibers and superplasticizer in HPC were 260 kg, 260 kg, 188 kg, 864 kg, 1024 kg, 1.8 kg and 4.1 kg per m^3 , respectively. Material properties of steel and concrete are listed in Tables 2 and 3. Construction drawings for the four specimens are shown in Fig. 1.

Table 1 Details of the specimens

Specimens	Concrete C50	Steel	Prestressing tendons	PPR	Top longitudinal reinforcements A'_s	Bottom longitudinal reinforcements A_s
PSRCB -1	HPC	With	2 - 4 ϕ^{P5}	0.75	2 Φ 12	2 Φ 12
PSRCB -2	HPC	With	2 ϕ^{S15}	0.85	2 Φ 12	2 Φ 12
SRCB	HPC	With	-	0	2 Φ 12	2 Φ 12
PHPCB	HPC	Without	1 ϕ^{S15}	0.75	2 Φ 12 + 2 Φ 18	2 Φ 12

Table 2 Material properties for steel

Material property	I-shaped steel	Steel bars			Steel wire	Steel strand
		$\phi 6$	$\phi 8$	$\phi 12$	ϕ^{P5}	ϕ^{S15}
Yield stress f_y (N/mm ²)	301.2	370.87	298.2	377.3	903.91	1740
Ultimate stress f_u (N/mm ²)	443.9	497.50	415.6	555.6	1802	1940
Modulus of elasticity E_s (N/mm ²)	1.9×10^5	2.11×10^5	2.02×10^5	1.88×10^5	1.90×10^5	-
Elongation ratio	27.78%	22.3 %	33.8%	23.3 %	7.0 %	5.5 %

Table 3 Material properties for concrete

Specimen	Cylinder compressive strength f_c (MPa)	Cube compressive strength f_{cu} (MPa)	Modulus of elasticity E_c (MPa)
PHPCB	39.60	52.11	3.58×10^4
SRCB	37.62	49.50	3.29×10^4
PSRCB-1	42.16	55.47	3.46×10^4
PSRCB-2	32.76	43.11	3.61×10^4

2.2 Testing

Beams were tested under two-point loading, which are shown in Fig. 2. The electrical resistance strain gauges, which were attached to steel bars, tendons, steel beams and concrete, were connected to a data acquisition system to record the data. Three displacement transducers were placed at the two supports and mid-span of each beam to measure the mid-span deflections. Fig. 3 depicts the arrangements of strain gauges and displacement transducers.

The vertical loading, simulating the seismic loads, were cyclically applied by using hydraulic actuators. The downward loads were applied first and all specimens were loaded to failure. Fig. 4 shows the loading history. The first cycle was load controlled, in which beams were loaded downwards until cracks formed at the bottom of pure bending sections of beams. The load corresponded to the concrete cracking was defined as P_{cr} . The subsequent cycles were displacement controlled. All beams were loaded three cycles in every levels of displacement. These displacements in successive sets of cycles, namely $+1\Delta_y$, $-1\Delta_y$, $+2\Delta_y$, $-2\Delta_y$, $+3\Delta_y$, $-3\Delta_y$,....., were multiples of Δ_y . Here, Δ_y was preliminarily determined based on the yielding of steel bars at bottom of pure bending sections and for comparison purpose, the yield displacement (Δ_y) was determined as 15 mm for PHPCB and 20 mm for the three SRC beams.

The followings were measured: (1) vertical loads; (2) mid-span and support deflections; (2) curvatures at mid-span sections; and (3) strains of steel bars, prestressing tendons and steel.

2.3. General observations and failure modes

1. Flexure cracks initiated at pure bending sections during the loading control stage. During the $+1\Delta_y$ and $-1\Delta_y$ load cycles, flexure-shear cracks could be observed and kept on propagating, thus penetrated over full depth of beam sections. As the load further increased, the existing cracks extended in terms of length and width without occurrence of new cracks. Finally, more vertical cracks and a few inclined cracks could be observed around mid-span sections of beams.

2. During the displacement control stage, crack widths and residual deformations of the prestressed SRC beams were obviously smaller than those of the nonprestressed SRC beam, showing that the prestressed SRC beams behaved relatively high crack closing and deformation restoring capacity.

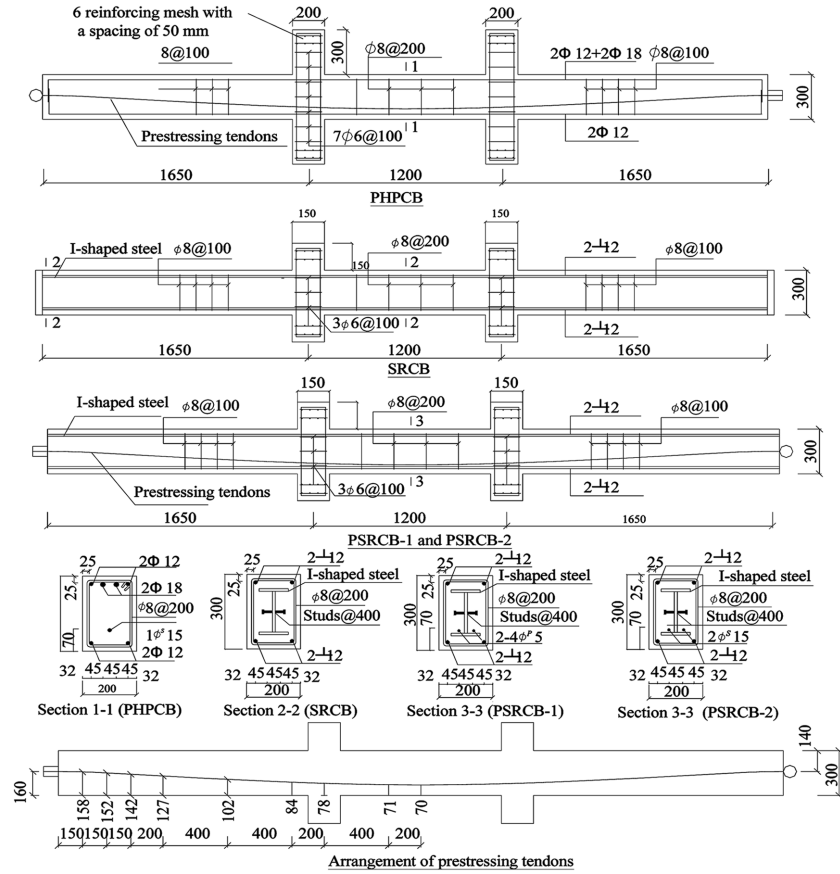


Fig. 1 Reinforcing details of the four beams

3. In loading cycles with a displacement of $2\Delta_y$ and subsequent cycles, all the SRC beams developed relatively high load-carrying capacity and loading stiffness.

4. All the specimens failed after undergoing large deformations. Concrete crushing along with buckling of longitudinal steel bars was observed on both top and bottom of PHPCB and PSRCB-2 at the pure bending section near the loading point. However, only the top concrete crushing accompanied by buckling of longitudinal steel bars was observed in SRCB and only the bottom concrete crushing and spalling off with buckling of longitudinal steel bars in PSRCB-1. These all showed that the failure of the four specimens was dominated by flexural effects. Fig. 5 depicts the failure modes of the four specimens.

3. Test results and analysis

3.1 Peak strains of bottom longitudinal steel bars, prestressing tendons, steel beams and studs in the four beams

Strains of bottom longitudinal steel bars, prestressing tendons, steel beams and studs in the four specimens were tested.

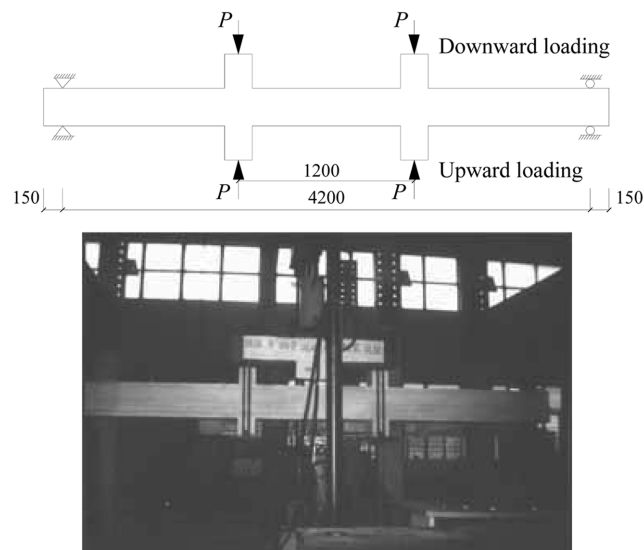


Fig. 2 Loading of beams

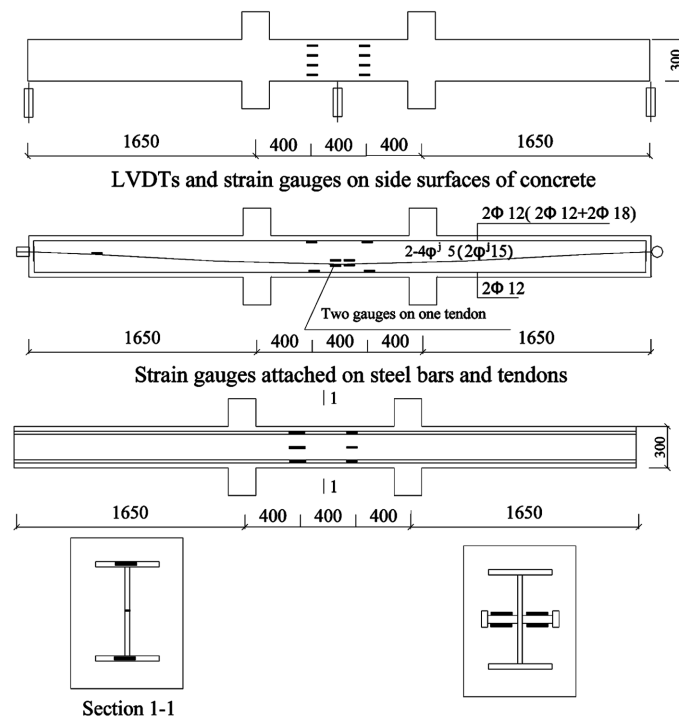


Fig. 3 Arrangements of strain gauges and displacement transducers

The peak strain was the maximum strain in load cycles with the same levels of displacement. As shown in Fig. 6, peak strains of the bottom longitudinal steel bars in all specimens varied little during

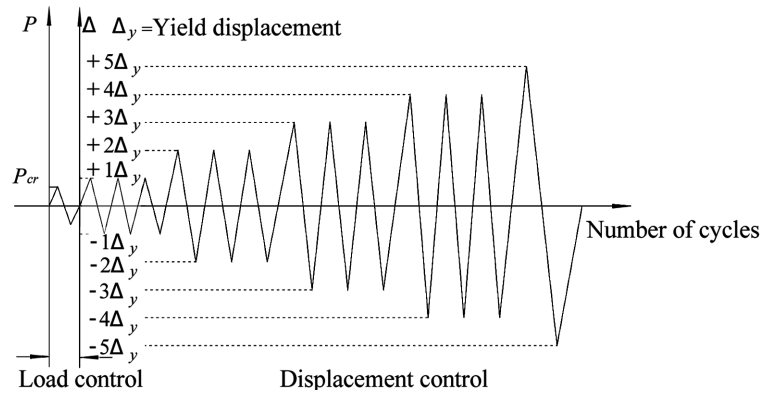


Fig. 4 Loading history

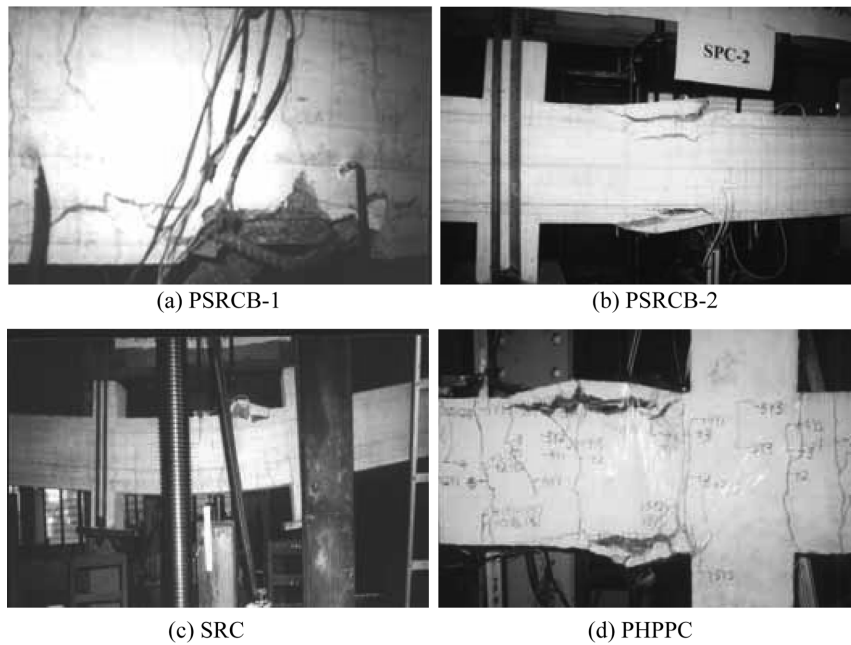


Fig. 5 Failure modes of the four beam specimens

upward loading. The reason was that the bottom longitudinal steel bars were under compression during upward loading. Peak strains of the bottom longitudinal steel bars in PHPCB increased about 300% in the $4\Delta_y$ load cycles during downward loading and those of the bottom longitudinal steel bars in the two prestressed SRC beams increased insignificantly with increase of load cycles. It could also be seen that the peak strains of the bottom longitudinal steel bars in SRCB were obviously larger than those in the prestressed SRC beams during downward loading. Moreover, peak strains of SRCB increased with increasing of levels of displacement during $+1\Delta_y$, $+2\Delta_y$ and $+3\Delta_y$ load cycles while almost kept constant during the $+4\Delta_y$ load cycles.

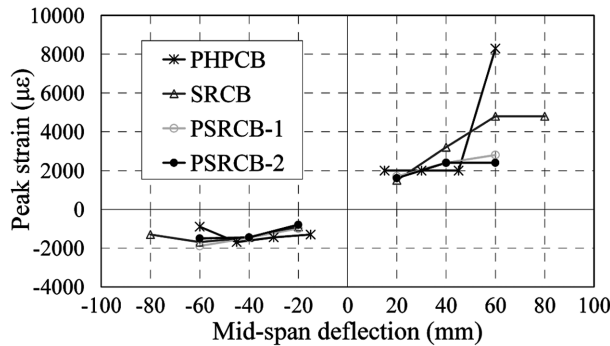


Fig. 6 Peak strain versus mid-span deflection curves for bottom longitudinal steel bars

As shown in Fig. 7, the difference between the total strain and the strain corresponding to the effective prestress level in the tendons after jacking was the strain increment. It was found that the peak strain increments of tendons in PHPCB were obviously higher than those in the two prestressed SRC beams during downward loading while lower during upward loading. The reason might be that the compression zone depth increased during both loading directions in the two prestressed SRC beams.

Fig. 8 showed that peak strains of steel beams in the three SRC beams were quite close and changed little in the $1\Delta_y$, $2\Delta_y$ and $3\Delta_y$ load cycles during both loading directions. However, there was a sharp increment in peak strains of steel beams in PSRCB-2 in the $4\Delta_y$ load cycles during downward loading, and peak strains of steel beam in PSRCB-2 were about 5 times of those of the other two beams at the last load cycles during downward loading.

As shown in Fig. 9, studs in the three SRC beams were under tension during the global testing. Peak strains of studs in these beams increased significantly in $2\Delta_y$ load cycles compared with those in the $1\Delta_y$ load cycles. Peak strains of studs in PSRCB-1 were lower than those in PSRCB-2 while greater than those in SRCB in load cycles with the same levels of displacement except in $4\Delta_y$ load cycles during downward loading. It could be observed that peak strains of studs in SRCB were quite close in the two loading directions, while the peak strains of studs in the two prestressed SRC beams during upward loading were about 2 times greater than those during downward loading. Tests also showed that prestressing led to increasing peak strains in studs.

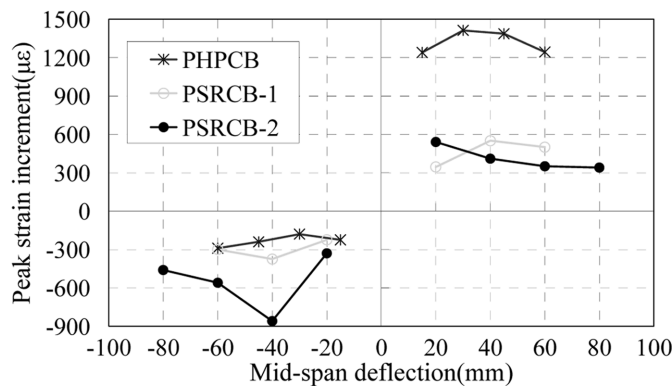


Fig. 7 Strain increment versus mid-span deflection curves for tendons and steel wires

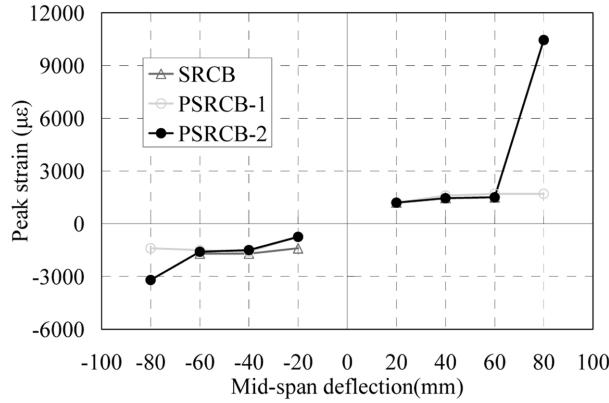


Fig. 8 Strain versus mid-span deflection curves for steel beams

3.2 Hysteresis curves

Hysteresis curves are load versus displacement relationships of beams under reversed cyclic loading, which can provide understandings for analysis of seismic elasto-plastic response. Hysteresis (P-Δ) curves of beams are shown in Fig. 10. Here, P is the applied vertical load at one of the two loading points and Δ is the mid-span deflection of each beam.

The followings can be observed from the above curves:

1. Obvious pinching could be observed in hysteresis loops of PHPCB as compared with those of the SRC beams. However, loops for the three SRC beams were obviously fuller, which showed that the SRC beams behaved relatively higher energy dissipation capacity. Moreover, two obvious pivot pinching points were observed in the hysteresis curves of the four specimens;
2. In load cycles with the same levels of displacement, the maximum loads obtained in the next two cycles were nearly the same as those in the first cycle, indicating that the load-carrying capacity of the four beams degraded little under reversed cyclic loading.
3. Hysteresis loops of the two prestressed SRC beams approached closely and were less full than those of SRCB. Compared with PHPCB, pinching was not so obvious in hysteresis loops of the prestressed SRC beams due to the effect of steel beams.

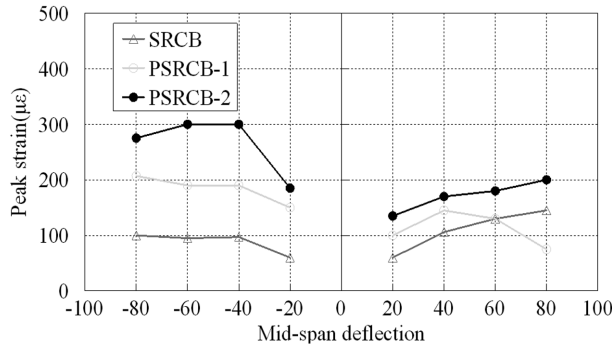


Fig. 9 Strain versus mid-span deflection curves for studs

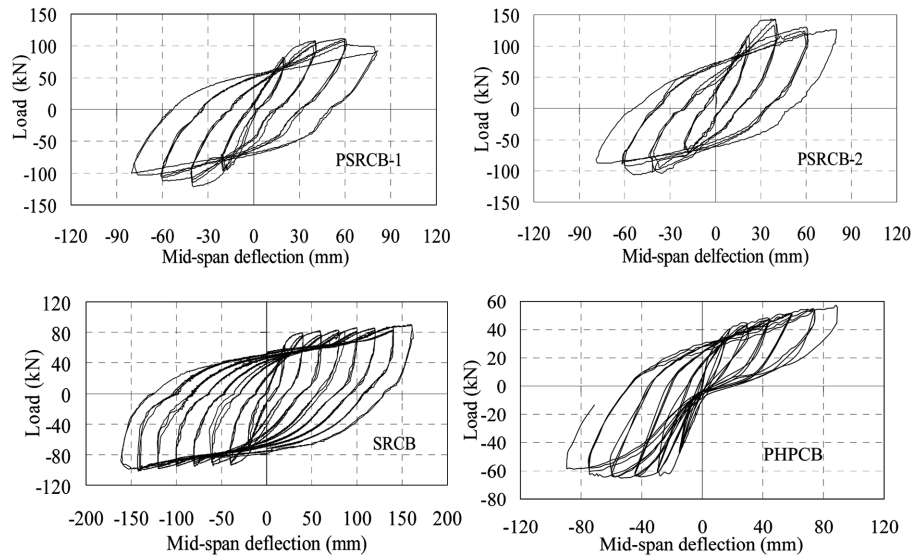


Fig. 10 Hysteresis curves for the four beams

4. An increment in load-carrying capacity of PSRCB-2 could be observed as compared with PSRCB-1 due to relatively high PPR.

5. The downward residual deformation for PHPCB was obviously smaller than that of the SRCB beams, indicating that the effect of prestressing in SRC beams was not so apparent as compared with that in PHPCB.

3.3 Skeleton curves

Skeleton curves for the four specimens are shown in Fig. 11. The followings could be observed from the curves:

1. All beams underwent the three stages: the elastic stage, the yield stage and the ultimate stage. Stiffness of these beams degraded obviously in all the stages.

2. Load-carrying capacity of PHPCB degraded at large displacement stage during upward loading. However, load-carrying capacity of SRCB beam specimen didn't degrade during both loading directions and the skeleton curves increased gradually, which showed that SRCB behaved relatively high displacement ductility. Upward load-carrying capacity of PSRCB-1 and PSRCB-2 degraded little during testing, while their downward load-carrying capacity degraded obviously.

3. Compared with PSRCB-1, PSRCB-2 showed higher downward load-carrying capacity due to a higher amount of prestressing tendons, but lower upward load-carrying capacity under the same levels of displacement which was attributed to the higher initial stress of the concrete within compression zone after jacking.

4. The yield point was quite obvious in skeleton curve of SRCB, while not so obvious in PSRCB-1 and PSRCB-2 due to the poor ductility of prestressing tendons.

5. Skeleton curves of the two prestressed SRC beams were quite similar. In comparison with SRCB, the load-carrying capacity of the prestressed SRC beams was obviously increased, accompanied by obviously decreased ultimate deformation which was quite close to that of PHPCB.

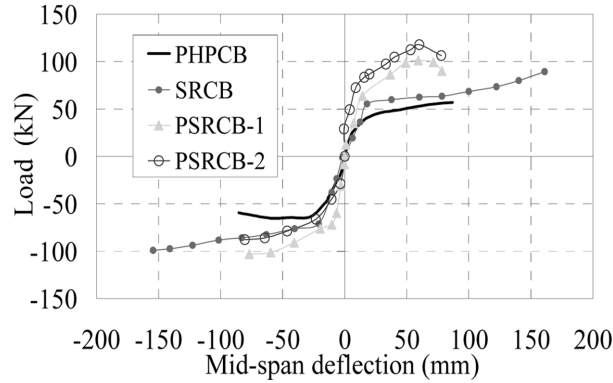


Fig. 11 Skeleton curves

3.4 Characteristic load

Characteristic loads for the four beams are presented in Table 4. Note that the cracking load was defined as the load corresponding to the first crack forming at the bottom of pure bending sections of beams and the yield load was defined as the load when the longitudinal steel bar yielded. It could be observed that cracking loads of the three prestressed beams were higher than that of SRCB during downward loading due to the effect of prestressing. Tests also showed that an increment in ultimate load-carrying capacity of the three SRC beams could be observed in comparison with that of PHPCB during both loading directions and the ultimate load-carrying capacity of the prestressed SRC beams was higher than that without prestressing during downward loading. A degradation of load-carrying capacity after maximum load point could be observed in the two prestressed SRC beams during downward loading, while that of the nonprestressed SRC beam and PHPCB degraded little.

3.5 Deformation restoring capacity

Deformation restoring capacity directly affects rehabilitation and serviceability of structures after earthquakes. In this paper, residual deformation ratio, which was defined as Δ_r / Δ_u , was used as a key index for evaluating deformation restoring capacity of beam specimens. Here, Δ_r was the residual displacement after unloading and Δ_u was equal to the maximum displacement for skeleton curves without descending branches or equal to the displacement corresponding to 85% maximum load in descending branch of the skeleton curves. Parameters for assessing restoring behaviors of the four beams are presented in Table 5.

Table 4 Characteristic loads for the four beams

Specimens	PHPCB		SRCB		PSRCB-1		PSRCB-2	
	↓	↑	↓	↑	↓	↑	↓	↑
Loading direction								
Cracking load P_{cr} (kN)	18.93	10.2	16.02	11.7	20.43	10.16	16.45	9.76
Yield load P_y (kN)	54.36	46.03	64.08	61.21	69.45	94.89	80.18	69.82
Maximum load P_{max} (kN)	61.08	65.30	94.24	99.11	102.13	103.07	102.79	87.99
Ultimate load P_u (kN)	-	-	-	-	90.90	-	92.51	-

As shown in Table 5, all the four specimens displayed relatively large deformation restoring capacity. The residual deformation ratio of PHPCB was about 0.33, which was obviously lower than those of the two prestressed SRC beams. The reason was that the steel beams encased in the concrete developed relatively large plastic deformations and hence increased the residual deformations of beams. The residual deformation ratios of the prestressed SRC beams were lower than that without prestressing due to the effect of prestressing. Tests also showed that PPR had little effect on the deformation restoring capacity by comparing the residual deformation ratios of PSRCB-1 and PSRCB-2.

3.6 Ductility coefficient

Displacement ductility is used as an important index for seismic evaluating of structures. The ductility coefficient μ , representing the ratio of ultimate displacement (Δ_u) to yield displacement (Δ_y) corresponding to the yield load, was defined as Δ_u / Δ_y . The measured ductility coefficients of the four beams are presented in Table 6.

It could be seen from the table that all the beam specimens behaved relatively ductile manners. The ductility coefficients of the two prestressed SRC beams and the prestressed concrete beam were 4.87, 4.65 and 4.79, respectively, implying that the steel beams exhibited little influence on the ductility. Of all the specimens, the nonprestressed SRC beam developed the most ductile manner with a ductility coefficient equal to 9.09, which was obviously higher than those of the prestressed SRC beams, so we could conclude that the prestressing in SRC beams would lead to a reduction in ductility of beams. In addition, the ductility coefficients of the prestressed SRC beams decreased with increasing PPR by comparing the ductility coefficients of PSRCB-1 and PSRCB-2.

3.7 Stiffness degradation

The stiffness, which was defined as $K = P/\Delta$, was used for describing stiffness degradation of specimens, where P was the applied vertical load at one of the two loading points and Δ was the mid-span deflection

Table 5 Parameters for deformation restoring capacity

Specimens	PHPCB		SRCB		PSRCB-1		PSRCB-2	
	↓	↑	↓	↑	↓	↑	↓	↑
Loading direction								
Residual deformation Δ_r (mm)	11.00	-48.40	129.19	-125.05	50.48	-53.76	49.78	-51.60
Ultimate deformation Δ_u (mm)	89.10	-89.50	160.82	-161.50	80.98	-80.22	80.07	-78.99
Residual deformation ratio Δ_r / Δ_u	0.12	0.54	0.80	0.77	0.62	0.67	0.62	0.65
	0.33		0.79		0.65		0.64	

Table 6 Ductility coefficients

Specimens	PHPCB		SRCB		PSRCB-1		PSRCB-2	
	↓	↑	↓	↑	↓	↑	↓	↑
Loading direction								
Cracking displacement Δ_{cr} (mm)	2.50	-1.50	2.29	-1.17	2.80	-0.88	3.03	-0.62
Yield displacement Δ_y (mm)	19.60	-17.8	17.13	-17.9	17.39	-17.38	17.97	-17.23
Ultimate displacement Δ_u (mm)	89.10	-89.5	158.92	-159.40	86.07	-83.00	81.61	-82.06
Ductility factor $\mu = \Delta_u / \Delta_y$	4.55	5.03	9.28	8.90	4.95	4.78	4.54	4.76
	4.79		9.09		4.87		4.65	

of the beam specimen. Fig. 12 shows the degradation of stiffness in the four beams. Obvious stiffness degradation of all the beams could be observed during the testing and mainly occurred from the loading stage corresponding to concrete cracking to that corresponding to yielding of beams. Stiffness of SRCB during upward loading was obviously larger than that during downward loading, which was similar to that of PSRCB-1 and PSRCB-2.

It could be seen from the figure that due to the effect of steel beams, the stiffness of PHPCB was lower than that of the SRC beams with the same levels of displacement during the whole loading stages. Initial stiffness of SRCB ranged from 5 to 6 kN/mm. An increasing initial stiffness ranging from 9 kN/mm to 10 kN/mm could be observed in prestressed SRC beams due to the effect of prestressing. The post-yield stiffness of the prestressed SRC beams was lower than that of SRCB, showing that the applied prestressing could result in an increase in cracking stiffness of the SRC beams, while had little effect on stiffness of these beams at large displacement stage.

3.8 Energy dissipation

The energy dissipation of the specimens under cyclic load in this study was defined as the area enclosed by the load-deflection hysteresis loop (Fang *et al.* 1994). The amount of energy dissipated by the four beams during testing is shown in Fig. 13.

Note that the amount of energy was average of every three load cycles under the same displacement. It could be found that the energy dissipation capacity of the beam specimens increased with increasing displacements. The vertical loads increased slowly and even decreased after beams were in elasto-plastic range due to cumulative damage. However, the energy dissipation capacity of beams still increased obviously at this stage. The amount of energy dissipated by PHPCB was obviously less than that dissipated by the three SRC beams. This resulted from the fact that the steel beams developed plastic deformations during large displacement stage in the SRC beams. The amount of energy dissipated by PHPCB was nearly the same in the two loading directions with identical levels of displacement. Energy that dissipated by SRCB during upward loading was obviously larger than that of during downward loading due mainly to the gravity loads. However, the amount of energy dissipated by the two prestressed SRC beams during upward loading was lower than that during downward loading. The attributed factors were that pinching occurred in hysteresis loops due to the effect of prestressing during downward unloading. Dissipation of energy increased slowly in PHPCB and even degraded at large displacement stage. By contrast, that kept on increasing in the three SRC beams at large displacement stage. Tests also showed

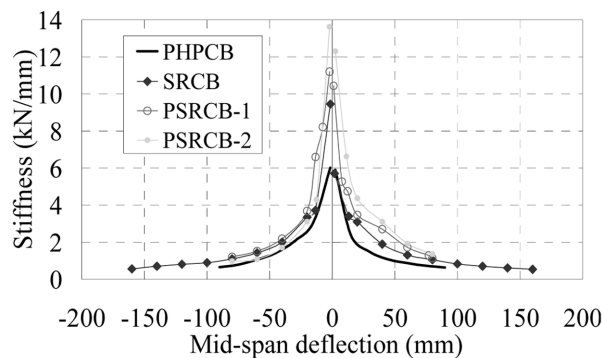


Fig. 12 Stiffness degradation

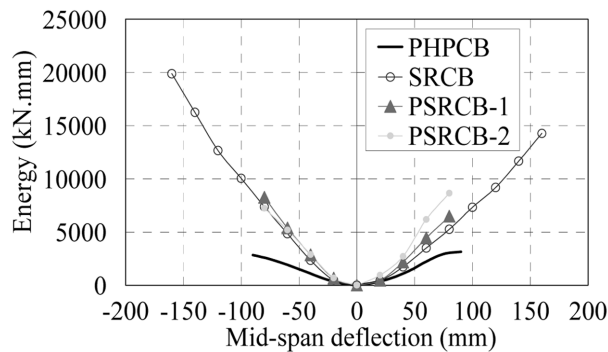


Fig. 13 Energy dissipation

that SRCB behaved the highest energy dissipation capacity among the four beams. The amount of energy dissipated by the two prestressed SRC beams during upward loading was quite close. However, more energy had been dissipated by PSRCB-2 as compared with that by PSRCB-1 during downward loading.

4. Conclusions

The following conclusions could be stated from the tests:

1. The failure modes for all specimens were dominated by flexural effects.
2. Hysteresis curves of the prestressed SRC beams were fuller than that of prestressed concrete beam, which showed that the prestressed SRC beams performed relatively high energy dissipation capacity. Obvious pinching could be observed in hysteresis loops of the prestressed concrete beam.
3. Little decrease in load-carrying capacity of the prestressed SRC beams occurred at large displacement stage during upward loading, however, obvious decrease in load-carrying capacity could be observed during downward loading. The opposite trend in load-carrying capacity was observed in the prestressed concrete beam. No decrease in load-carrying capacity of nonprestressed SRC beam during both loading directions occurred.
4. Residual deformation ratios of the two prestressed SRC and nonprestressed SRC beams were 0.65, 0.640 and 0.79, respectively, implying that the prestressed SRC beams behaved relatively higher deformation restoring capacity. Residual deformation ratio of the prestressed concrete beam was about 0.33 which was obviously lower than those of the prestressed SRC beams, indicating that the plastic deformations of steel beams had a significant effect on the residual deformations of prestressed SRC beams.
5. The ductility coefficients of the prestressed SRC beams and the prestressed concrete beam ranged between 4.65 and 4.87, which were obviously lower than that of nonprestressed SRC beam (9.09), indicating the steel beams influenced the ductility little while prestressing resulted in a reduction in ductility.
6. Obvious stiffness degradation of the four beams could be observed during the testing and mainly occurred from the loading stage corresponding to concrete cracking to that corresponding to yielding of the beams. The applied prestressing could result in an increase in initial stiffness of the SRC beams while had little effect on stiffness of these beams at large displacement stage.
7. Compared with the prestressed SRC beams and the prestressed high performance concrete beam, more energy was dissipated by the nonprestressed SRC beam. At large displacement stage, dissipation of energy increased slowly in PHPCB, while kept on increasing gradually in the SRC beams.

References

- Azizinamini, A. and Ghosh, S. K. (1997), "Steel reinforced concrete structures in 1995 Hyogoken-Nanbu Earthquake", *J. Struct. Eng. ASCE*, **123**, 986-992.
- Chen, C.C. and Lin, K.T. (2008), "Behavior and strength of steel reinforced concrete beam-column joints with two-side force inputs", *J. Constr. steel res.*, doi:10.1016/j.jcsr.2008.03.010.
- Cheng, C. T. and Chung, L. L. (2002), "Seismic performance of steel beams to concrete-filled steel tubular column connections", *J. Constr. steel res.*, **59**, 405-426.
- Chou, C. C. and Uang, C. M. (2001), "Cyclic performance of a type of steel beam to steel-encased reinforced concrete column moment connection", *J. Constr. steel res.*, **58**, 637-663.
- Fang, I. K., Wang, C. S. and Hong, K. L. (1994), "Cyclic Behavior of High-Strength Concrete Short Beams with Low Amount of Flexural Reinforcement", *ACI Struct. J.*, **91**(1), 10-18.
- Lee, T. K. and Pan, A. D. E. (2001), "Analysis of composite beam-columns under lateral cyclic loading", *J. Struct. Eng. ASCE*, **127**, 186-193.
- Lu, W. Y. (2006), "Shear strength prediction for steel reinforced concrete deep beams", *J. Constr. steel res.*, **62**, 933-942.
- Sun, G. C., Zhang, J. W. and Chen, Q. (1996), "Design methods for prestressed steel reinforced concrete beams", *Jiangsu Architec*, **4**, 25-28. (in Chinese)
- Teraoka, M., Morita, K., Sasaki, S. and Katsura, D. (2001), "Experiment study on simplified steel reinforced concrete beam-column joints in construction technology", *Steel Compos. Struct.*, **1**(3), 295-312.
- Wakabayashi, M. (1986), *Design of earthquake-resistant buildings*, McGraw, Newyork.
- Xue, J. Y. and Zhao, H. T. (2000), "Elasto-plastic analysis of seismic responses for steel reinforced concrete frame model", *Journal of Building Structures*, **21**(4), 28-33. (in Chinese)